International Journal of Thermal Sciences 124 (2018) 23–35

Contents lists available at ScienceDirect

International Journal of Thermal Sciences

journal homepage: www.elsevier.com/locate/ijts

Thermal management of lithium ion batteries using graphene coated nickel foam saturated with phase change materials

Abid Hussain[a], Irfan H. Abidi[b], C.Y. Tso[a,c], K.C. Chan[a,d], Zhengtang Luo[b], Christopher Y.H. Chao[a,*]

[a] Department of Mechanical and Aerospace Engineering, The Hong Kong University of Science and Technology, Clear Water Bay, Kowloon, Hong Kong, China
[b] Department of Chemical and Biomolecular Engineering, The Hong Kong University of Science and Technology, Clear Water Bay, Kowloon, Hong Kong, China
[c] HKUST Jockey Club Institute for Advanced Study, The Hong Kong University of Science and Technology, Clear Water Bay, Kowloon, Hong Kong, China
[d] Fok Ying Tung Graduate School, The Hong Kong University of Science and Technology, Clear Water Bay, Kowloon, Hong Kong, China

ARTICLE INFO

Keywords:
Graphene coated nickel foam
Lithium ion batteries
Phase change material
Passive thermal management
Thermal conductivity

ABSTRACT

Lithium ion (Li-ion) batteries are an integral part of electric vehicles and hybrid electric vehicles because of their high energy and power density. These batteries suffer from a high temperature rise during operation, thus affecting their life span and efficiency. In this study, thermal management of Li-ion batteries was accomplished by using a novel material (Graphene coated nickel (GcN) foam saturated with paraffin). The growth of graphene coated on nickel foam was carried out using chemical vapor deposition. The thermal conductivity of the pure paraffin wax was enhanced by 23 times after infiltrating it into the GcN foam. The paraffin was used as a phase change material (PCM). The melting and freezing temperatures of the GcN foam saturated with paraffin were increased and decreased respectively as compared to pure paraffin. The latent heat and specific heat of the GcN foam saturated with paraffin is decreased by 30% and 34% respectively as compared to pure paraffin. The thermal management for Li-ion batteries is also compared among five materials: nickel foam, paraffin wax, GcN foam, nickel foam saturated with paraffin and GcN foam saturated with paraffin. The battery surface temperature rise is 17% less using graphene coated nickel foam saturated with PCM as compared to using nickel foam under 1.7 A discharge current.

1. Introduction

Electric vehicles (EVs) and Hybrid electric vehicles (HEVs) are a developing market and an attractive substitute for traditional vehicles, particularly because of their lower environmental hazards and fuel intake [1]. However, there are still some specialized developments required to make EVs and HEVs more effective and attractive for purchasers. Cost, weight, battery life and driving range are a few of the foremost problems with HEVs and EVs [2]. Lithium ion (Li-ion) batteries have become an integral part of HEVs and EVs due to their prolonged life and high energy density [3]. Li-ion batteries generate excessive heat during operation due to their high power and energy densities. There is a requirement for efficient and compact thermal management systems (TMSs) to manage their extreme temperature upsurge. Active TMS [4,5] and passive TMS [6,7] are two popular thermal management techniques.

Tran et al. designed heat pipe modules for thermal management of lithium ion batteries [8]. They found that the heat pipe coupled with different ventilation arrangements proved to be a favorable thermal management solution for HEV batteries. Greco et al. developed a 1-D transient model combining a thermal heat pipe model with a thermal circuit [9]. They proved that the temperature of the lithium ion batteries dropped from 52 °C to 28 °C by using the 1-D transient model. Mohammadian et al. embedded aluminum foam into the heat sink to cool the lithium ion batteries [10]. They found that the surface temperature of lithium ion batteries was significantly reduced after using aluminum foam inside the heat sink as compared to the case without aluminum foam. Zhao et al. used a liquid cooled cylinder to cool lithium ion batteries [11]. They found that the surface temperature of 42 cylindrical batteries was kept under 40 °C by use of a liquid cylinder. All the active cooling approaches mentioned above are expensive due to the addition of heat pumps, heat sinks, fan components, etc.

An alternative technique, passive thermal management (e.g. a phase change material), has become an attractive approach in recent years as it is highly efficient, compact and lightweight. Phase change materials (PCMs) store thermal heat in the form of sensible and latent heat,

* Corresponding author. Department of Mechanical and Aerospace Engineering, Main Academic Building, The Hong Kong University of Science and Technology, Clear Water Bay, Kowloon, Hong Kong, China.
E-mail address: meyhchao@ust.hk (C.Y.H. Chao).

http://dx.doi.org/10.1016/j.ijthermalsci.2017.09.019
Received 15 May 2017; Received in revised form 12 September 2017; Accepted 28 September 2017

Nomenclature

c_p	Specific heat capacity [J/(g.K)]
d	Thickness [m]
E	DSC calorimetric sensitivity
H	Enthalpy [J/kg]
k	Thermal conductivity [W/(m.K)]
M	Mass [kg]
r	Radius [m]
T	Temperature [°C]
t	Time [s]
V	Volume [m^3]

Greek symbols

α	Thermal diffusivity [m^2/s]
β	Impregnation ratio [-]
ε	Porosity [-]
ω	Pore density [PPI]
γ	Surface energy [J/m^2]
ρ	Density [kg/m^3]

Subscript

f	Fluid
l	Liquid
m	Melting
s	Solid

Abbreviations

A	Ampere
Ah	Ampere-hour
C	Charge/discharge rate
CVD	Chemical vapor deposition
DAQ	Data acquisition system
DSC	Differential scanning calorimeter
EV	Electric vehicle
GcN	Graphene coated nickel
HEV	Hybrid electric vehicle
PCM	Phase change material
PPI	Pores per inch
RT	Rubitherm
S	Series

mainly in the latent heat form due to the large latent storage capacity i.e. water, paraffin wax, etc. PCM changes state from solid to liquid or liquid to gas or vice versa at almost constant temperature during latent heat storage. PCMs classified as TMSs should be low cost, non-corrosive and with large latent heat [12]. PCMs also have benefits over other storage materials (e.g. refrigerants, water, glycol, oil, etc.) due to their low volume expansion, being non-poisonous and non-explosive nature [13]. It is also worth mentioning that common PCMs suffer from very low thermal conductivity (~0.1–0.3 W/(m.K)) [12]. The heat storage rate is affected by the low thermal conductivity of the PCMs. Many techniques have been mentioned in the literature to improve the thermal conductivity of PCMs. Goli et al. used graphene-paraffin composite to improve the thermal conductivity of a pure PCM [14]. They found that thermal conductivity of a graphene/paraffin composite reached 45 W/(m.K) as compared to 0.2 W/(m.K) of pure paraffin. They also observed that temperature rise of the lithium ion batteries using graphene/paraffin composite was 16 °C as compared to 37 °C with no graphene/paraffin wax composite under a 5A discharge current. Kizilel et al. used a graphite matrix to increase the thermal conductivity of paraffin [15]. They observed that the paraffin-graphite matrix had a thermal conductivity of about 17 W/(m.K). They found that hybrid PCM facilitates a uniform temperature for lithium ion batteries under normal and stressed conditions. Aadmi et al. enhanced the thermal conductivity of epoxy resin by 3–4 times by loading the paraffin wax inside metal hollow tubes [16]. They found that a higher energy storage capacity and lower temperature rise can be obtained by increasing the paraffin wax content in the composite. Zhang et al. used graphite nanoplatelets (GnPs) and found that the thermal conductivity of polyethylene glycol was enhanced by 9 times at 8% GnP mass ratio [17]. They also observed that the latent heat of the composite decreased as the concentration of GnP increased. Microcapsules, carbon fibers and nanoparticles have also been used to increase the thermal conductivity of paraffin wax as a PCM [18–20].

Metal foams have also been proven to be a viable option in enhancing thermal conductivity of PCMs. High porosity, good thermophysical properties and mechanical strength are salient features of metal foams. Li et al. [21] utilized a copper foam-paraffin wax composite to study the performance of the thermal management system of a 10 Ah Li-ion battery pack. They compared the result with two modes: natural air convection and pure paraffin. The battery surface temperature was 29% and 12% lower after using copper foam-paraffin wax composite as the thermal management source as compared to the air convection mode and the pure paraffin respectively under 1C discharge rate. Hussain et al. used a nickel foam-paraffin composite to experimentally investigate the battery surface temperature of a 3.4 Ah lithium ion battery pack [22]. They found a decline in battery surface temperature by 31% and 24% as compared to natural air and pure paraffin mode respectively under 2C discharge rate. Samimi et al. observed a drop of 15 °C in battery surface temperature after using a carbon fiber-paraffin wax composite [23]. They obtained an increase of 81–273% in thermal conductivity of composite material as compared to pure paraffin. Sabbah et al. utilized graphite to enhance the thermal conductivity of paraffin wax [24]. They treated an electric heater as a battery. They found that heater surface temperature was 5% lower by

Table 1
Summary of metal foams used to enhance thermal conductivity of paraffin wax.

	Metal foam	Paraffin melting temp. (°C)	Thermal conductivity of pure paraffin W/(m.K)	Thermal conductivity of metal foam-paraffin composites W/(m.K)	Nature of measurement
Khateeb et al. [25]	Aluminum	41–44	0.2	44	Theoretical
Wang et al. [46]	Aluminum	46–52	0.2	46	Theoretical
Li et al. [21]	Copper	42–49	0.2	11	Theoretical
Xiao et al. [27]	Copper	60–62	0.3	5	Experimental
Hussain et al. [22]	Nickel	38–41	0.2	2	Theoretical
Xiao et al. [47]	Nickel	60–62	0.4	2	Experimental
Ji et al. [48]	Ultrathin-graphite	58.9	0.2	4	Experimental
Sabbah et al. [24]	Expanded Graphite	52–55	N.A.	17	Theoretical
Fathabadi [49]	Expanded Graphite	58–60	0.2	17	Theoretical

employing graphite-PCM composite. Khateeb et al. used aluminum foam to improve the thermal conductivity of paraffin wax [25]. They found that the surface temperature of a 13.2 Ah battery was 5% lower as compared to paraffin wax. Studies regarding thermal conductivity enhancement of PCM based on metal foam-PCM composites are summarized in Table 1.

In previous studies, the thermal management of lithium ion batteries was mainly carried out using either graphene-paraffin composite or metal foam (copper, nickel or aluminum)/paraffin composite. The thermal conductivity of graphene is very high (~2000–3000 W/(m.K)) [33,34]. The thermal conductivity of paraffin wax has been increased after being infiltrated into nickel foam and graphene coated nickel foam. But the problem is that the nickel foam enhances the thermal conductivity of paraffin only six times [27] and the thermo-mechanical properties (such as tensile strength and compressive strength) of graphene-paraffin composite become weaker at elevated temperatures [6]. Herein, the use of graphene coated nickel foam as a thermal management system for lithium ion batteries is reported. In this study, thermal management of lithium ion batteries was carried out using a new thermal management material (combination of graphene, metal (nickel) foam and paraffin wax). The advantages of using nickel are numerous: corrosion resistance, high specific strength and toughness

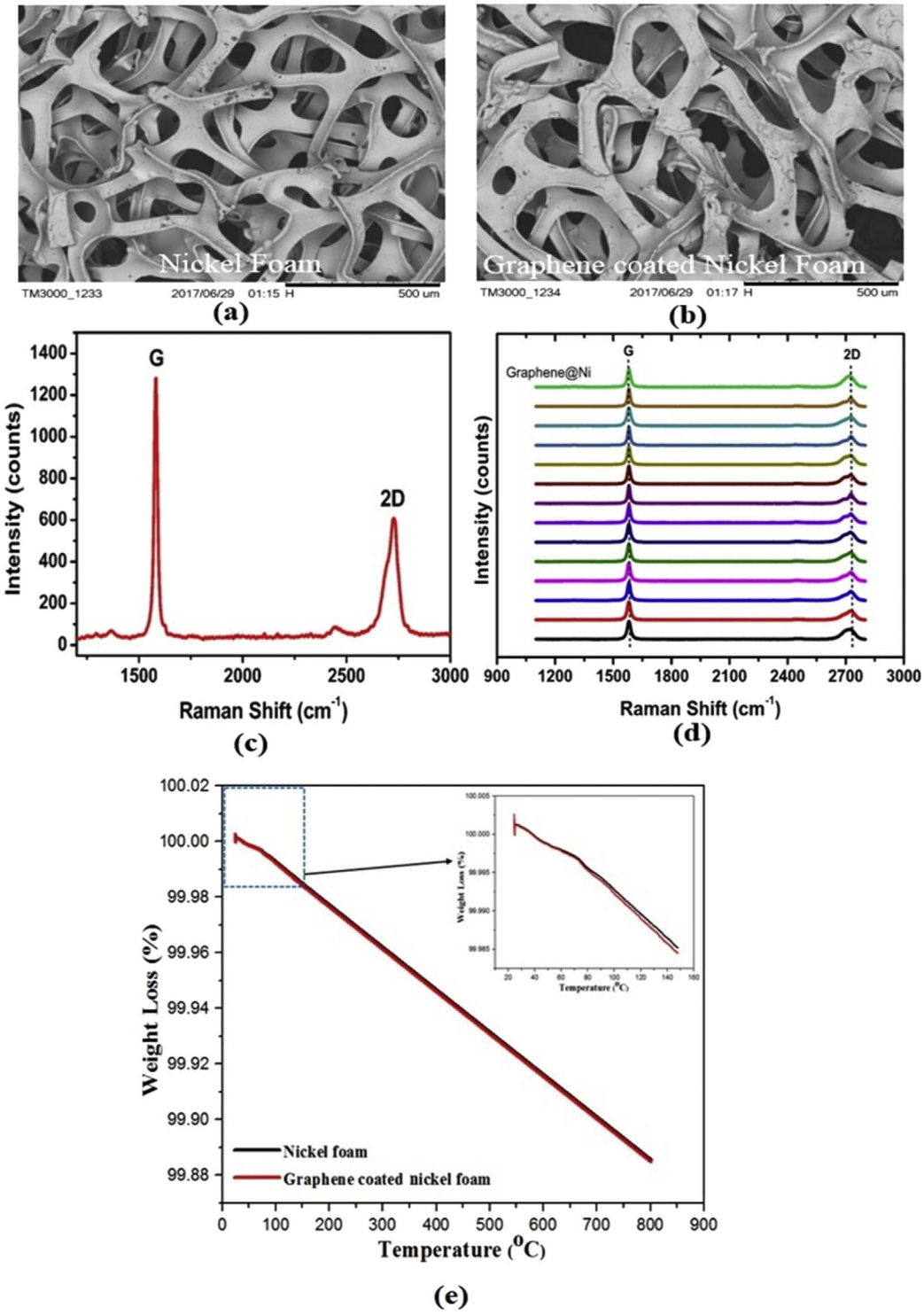

Fig. 1. Graphene coated nickel foam. (a) Scanning electron microscopy image of nickel foam (b) Scanning electron microscopy image of graphene coated nickel foam (c) Raman spectrum of the graphene coated nickel foam (d) Raman spectra acquired from 14 random spots of the composite substrate (e) TGA analysis of nickel and graphene coated nickel foam.

[26] and the mechanical properties of nickel can be improved by strengthening the nickel with fibers/particles [27]. Carbon atoms can be easily dissolved in nickel due to their high solubility in nickel [28] and the nickel surface can also be easily pre-patterned so that the graphene patterns of preferred geometries can be produced meticulously [29]. Nickel foam is suitable for graphene synthesis, if a few layers of graphene are deposited [30]. Graphene shows exceptional compatibility with a range of porous materials [31,32]. Graphene based composites have superior mechanical properties over the composite itself [31] and have a low coefficient of thermal expansion [32,33]. Zhao et al. reported that the Young's modulus and mechanical properties of the composite (poly(vinyl alcohol) and graphene nanosheets) are increased by about 10 times and 150% at 2 vol.% graphene loading in composite material [31]. Graphene growth on nickel foam will make the GcN foam harder (Ni foam becomes 1.2 times harder with the addition of 0.05 g/L graphene) [35]. The cycling performance of GcN foam is outstanding (capacitance retention of 98% after 10000 cycles at 3 mA/cm) [36].

The objective of this study was to investigate the performance of the thermal management system of lithium ion batteries based on graphene coated nickel foam saturated with paraffin wax. Four other thermal management materials i.e. nickel foam, paraffin wax, graphene coated nickel foam and nickel foam saturated with paraffin wax were also studied and compared with each other. Additionally, the performance of GcN foam saturated with paraffin wax as a thermal management material at higher operating conditions (30 °C, 33 °C) were also studied. Further, the thermal characterization (thermal conductivity, latent heat, phase change temperature and specific heat capacity) of graphene coated nickel (GcN) foam saturated with paraffin wax was also included in this study. The results were compared with pure paraffin wax and nickel foam saturated with paraffin wax.

2. Preparation and characterization of graphene coated nickel foam

The nickel foam ($\varepsilon = 0.9$, $\omega = 0.5$ mm (12.7 PPI)) was provided by Zhenjiang Global Industrial Components Trading Co. Ltd. China. The nickel foam was cut to the particular size (58 mm × 65 mm x 1.7 mm) to match the size of the individual battery cells then ultrasonically cleaned with acetone and dried under nitrogen. The nickel foam pieces were loaded into a chemical vapor deposition (CVD) reaction chamber (i.e. tube furnace with a sliding chamber to achieve fast heating and cooling rates). The graphene coating on the nickel foam was achieved by heating the furnace to graphene growth conditions. The temperature for growth is 900 °C under the flow of argon (Ar) at 200 standard cubic centimeters per minute (sccm) and hydrogen at 100 sccm. The nickel foam samples were annealed at that temperature for 30 min, followed by the introduction of a carbon precursor (ethylene) at a flow rate of 5 sccm for 10 min to obtain a few layers of graphene coating on the nickel foam. After that, the system was rapidly cooled by switching off the furnace. Fig. 1 (a and b) display the scanning electron microscopy (SEM) images of the nickel foam and graphene coated nickel foam respectively. The amount of graphene loading was estimated with the number of graphene layers which was determined through Raman spectroscopy. The Raman spectrum shown in Fig. 1 (c) corresponds to 3–5 layers of graphene according to the literature [37]. The thickness of the few (3–5) graphene layers on the nickel foam could be 1–2 nm [38]. The mass percentage of graphene in the graphene coated nickel foam is around 0.5%. The mass percentage of graphene on graphene coated nickel foam was determined by measuring the mass of the nickel foam before and after coating the nickel foam with graphene.

The growth of graphene on the nickel foam was monitored using micro-Raman spectroscopy as shown in Fig. 1 (c). Raman analysis was carried out using an In-Via micro Raman system (Renishaw) equipped with Ar + ion laser 514 nm. A 50X objective lens was used to focus the laser beam. The laser power at the sample surface was 3 mW. The ratio of the G band to 2D band (> 1) reflects the few layers of graphene coating on the nickel foam. The defect free graphene growth was evident by the two peaks at 1585/cm and 2731/cm [38]. As the CVD growth process is a gas phase reaction, it can be speculated that the distribution of ethylene among the nickel foam is uniform as in the case for graphene distribution. Besides, Raman analysis of graphene loaded Ni foam at various random points was also carried out to confirm that the graphene was uniformly distributed on the nickel substrate. Raman spectra were acquired from 14 random spots of the composite substrate, and each spectra shows typical features of few layer graphene which reflects a uniform distribution of graphene in the composite as shown in Fig. 1 (d). Moreover, a thermogravimetric analysis (TGA) method was carried out to examine the thermal stability of the graphene coated nickel foam. TGA was carried out using Q5000 under a nitrogen atmosphere of 25 ml/min and the heating rate was maintained at 2 °C/min. There was no significant decomposition of either the nickel foam or the graphene coated nickel foam with the rise of temperature. A small mass difference (0.1%) exists between the nickel foam and after coating the nickel foam with graphene on close examination, which suggests that nickel foam and graphene coated nickel foam are thermally stable even at temperatures as high as 900 °C. The TGA analysis for the metal foams is shown in Fig. 1 (e).

3. Thermo-physical characterization of metal (nickel/graphene coated nickel) foam/paraffin composites

3.1. Thermal conductivity measurement

The thermal diffusivities of the nickel foam saturated with paraffin wax and the graphene coated nickel foam saturated with paraffin wax were measured at an ambient temperature of 25 °C using an instrument designed on the basis of the flash method technique. The dimensions of each sample (nickel foam saturated with paraffin wax and graphene coated nickel foam saturated with paraffin wax) were 60 mm × 25 mm x 1.7 mm. The top surface of each sample was attached to a metal rod. This thermal contact was made tight by using a thermal interface material (thermal tape) to reduce the contact resistance. An electric heater was used to raise the temperature of the metal rod. The temperature of the metal rod was maintained at 35 °C, monitored by an IR detector (FLIR SC660). The experimental setup to measure thermal diffusivity of nickel foam saturated with paraffin wax and graphene coated nickel foam saturated with paraffin wax is shown in Fig. 2 (a). The temperatures of the samples were monitored and recorded at three points (point 1 is at a distance of 6 mm from the top, point 2 is in the center at a distance of 30 mm from the top and point 3 is at a distance of 54 mm from the top) by IR detector as shown in Fig. 2 (b). The time in which the temperature rise on the back face of the sample reaches one half of its maximum value, $t_{1/2}$, was measured from the experiment. The rate of heat transmission by conduction during variations of temperature with time is called thermal diffusivity (α). The temperature rise against time is used for measuring the thermal diffusivity by the following equation [39]:

$$\alpha = \frac{1.38d^2}{\pi^2 t_{\frac{1}{2}}}, \tag{1}$$

where α is the thermal diffusivity (m^2/s), d is the length of the sample (m) through which heat flows and $t_{1/2}$ is the time to the half maximum (s). The value of l in this case is 60 mm. The thermal conductivity, k, was then estimated by using the following equation.

$$k = \alpha \rho c_p, \tag{2}$$

where k is thermal conductivity (W/(m.K)), α is the thermal diffusivity (m^2/s), and ρ is the density of the samples (kg/m^3) obtained by dividing the mass of the samples by their respective volume. The masses of the composites were measured using an electronic precision balance and

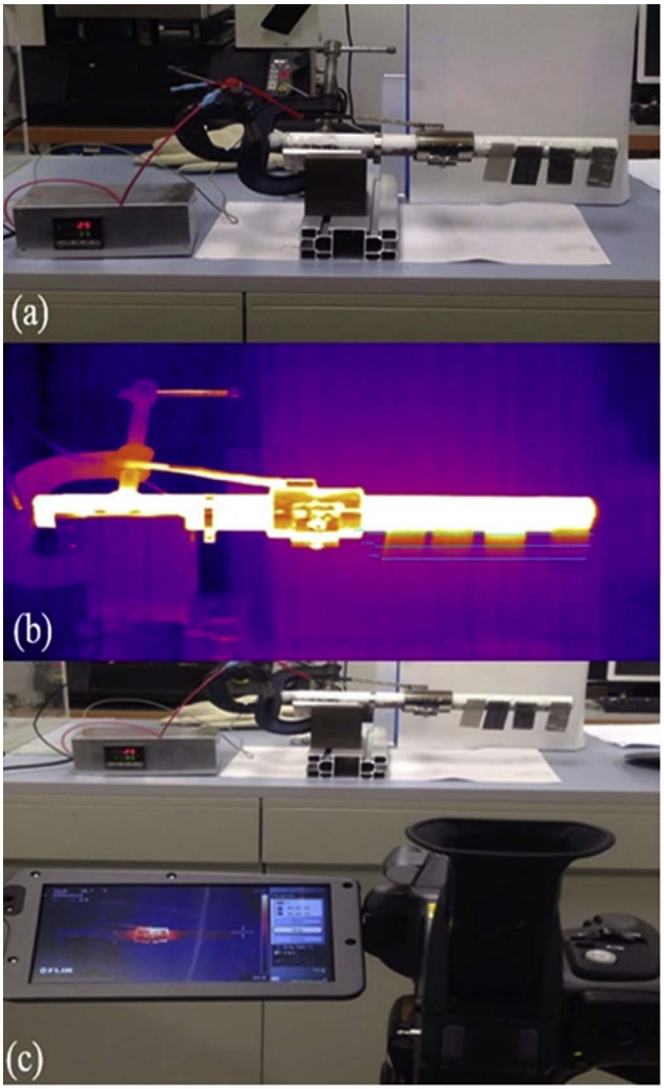

Fig. 2. Experimental setup to measure the thermal diffusivity of nickel foam saturated with paraffin wax and graphene coated nickel foam saturated with paraffin wax.

volumes were obtained by multiplying dimensions (L x W x H) of the samples as after infiltrating paraffin, the porous metal foam became a solid rectangular structure. The c_p in equation (2) is the specific heat capacity of the samples (J/(g.K)). The specific heat capacity of the composites was measured using a differential scanning calorimeter (DSC) Q1000 under a nitrogen atmosphere of 50 ml/min and the heating and cooling scanning rates were maintained at 2 °C/min. The samples were cooled from 60 °C to 5 °C during the first scanning and after that the samples were allowed to reach the equilibrium state by programming a 5 min isothermal segment. After that, the heating segment was carried out from 5 °C to 60 °C. The mass of the samples was kept constant during the DSC tests. DSC calorimetric sensitivity was obtained by performing a base line test without a sample and standard tests with standard materials (i.e. aluminum, platinum). DSC tests for the samples were then made. The specific heat capacities of the samples were determined using the following.

$$c_p = \frac{E_{sample} - E_{base\ line}}{M_{sample} \cdot \ {}^{dT}/_{dt} \cdot \ E}, \tag{3}$$

where M_{sample} is the mass of the sample, E is the DSC calorimetric sensitivity and is determined by the following equation.

$$E = \frac{E_{standard} - E_{base\ line}}{M_{standard} \cdot \ {}^{dT}/_{dt} \cdot \ c_{p\ standard}}, \tag{4}$$

$M_{standard}$ is the mass of the standard material and ${}^{dT}/_{dt}$ denotes the scanning rate. The uncertainty in c_p measurements is 5.4%. The temperature sensitivity and accuracy of the IR camera are 0.05 °C and ± 1 °C respectively. The repeatability and accuracy of the results were ensured by repeating the experiments 6 times. The uncertainty arising due to thickness measurement of the samples was estimated to be 0.1%. The uncertainty in temperature measurement was estimated to be 1.2%. The uncertainty resulting from the heater pulse time effect was estimated to be 1.6%. A 3% uncertainty due to the effect of non-uniform heating was estimated. In all cases, the influence of heat losses on the thermal diffusivity accuracy was estimated at 2%. The uncertainty in density measurement of the samples was estimated to be 0.6%. The uncertainty in the measurement of the specific heat was estimated to be 5.4%. Overall, the uncertainty in the thermal conductivity determination was 14%.

3.2. Differential scanning calorimeter (DSC) measurements

Latent heat is an important parameter to characterize the phase change behavior of the pure paraffin and metal foam/paraffin composites. This parameter was measured by the DSC Q1000 (TA instrument) in the present study and its temperature accuracy was within 0.2 °C ± 1%. The samples were sealed in a standard aluminum pan by the sample fastening assembly. Both the sample pan and reference pan were put into the furnace. The amount of samples analyzed ranged from 2.3 to 2.7 mg. DSC measurements were carried out under a nitrogen flow of 50 ml/min and temperature range of 0–60 °C. All samples were subjected to freezing-melting cycles with a cooling and heating rate of 2 °C/min. The specific heat capacity was measured by comparing the temperature rise of the sample to that of the reference pan using the DSC Q1000 (TA instrument) equipment. The reference pan was an empty aluminum pan with no sample, so that the effect of the aluminum pan holding the sample can be eliminated. The specific heat capacity, c_p, of the reference pan is ~0.9 J/(g.K) at 25 °C. The uncertainty of the temperature (melting phase and freezing phase) measurement from the DSC machine is 0.2 °C ± 1%.

4. Experimental setup

4.1. Preparation of battery packs

Commercial Type (Panasonic NCR18650B) Lithium-ion battery cells with a capacity of 3400 mAh were used. Each cell was initially tested at a charge and discharge rate of C/2 to check for the rated capacity. The cells, whose nominal capacity was above 90%, were used to build the battery pack. The details of electrical characteristics of the battery cell are listed in Table 2. The battery pack configuration was 6S (six cells in series) with capacity of 3.4 Ah. The connection bars used to construct the battery pack are curved in nature to avoid the short circuit chances. Moreover, safety circuit was connected with battery pack to prevent overcharging or short circuit and to adjust the pack voltage of discrete cells as shown in Fig. 3 (b).

The battery pack specification is summarized in Table 3.

The paraffin wax (Rubitherm 42) was provided by Ruhr Energy

Table 2
Electrical characteristics of battery cell.

Cell type	Panasonic NCR18650B
Nominal voltage (V)	3.7
Cell capacity (Ah)	3.4
Operating voltage (V)	3.0–4.1
Cell height (mm)	65
Cell diameter (mm)	18.4

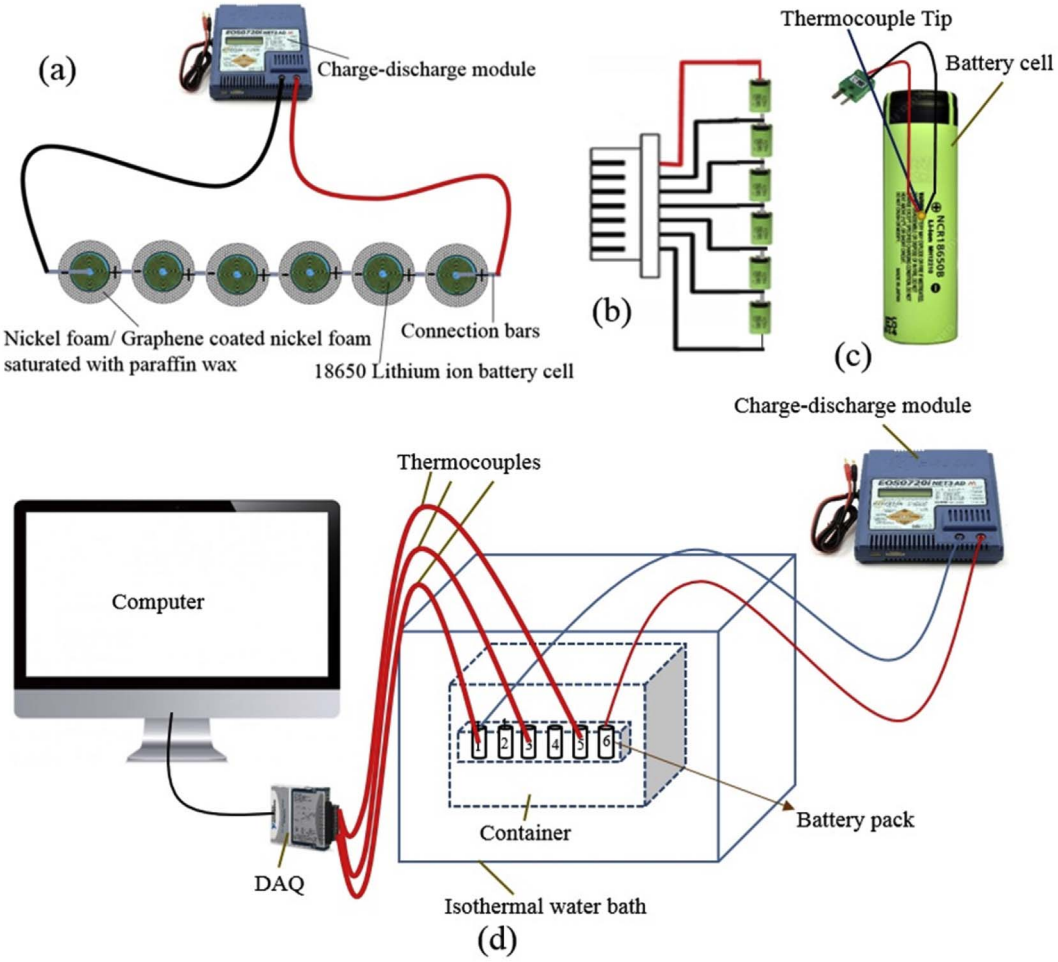

Fig. 3. (a) Schematic diagram of battery cells wrapped with metal foam/PCM (b) Schematic diagram of cell balancing (c) location of thermocouple on battery cell (d) Schematic diagram of experimental setup for passive thermal management of lithium ion batteries.

Table 3
Electrical characteristics of battery pack.

Cell configuration	6S
Pack capacity (Ah)	3.4
Spacing between cells (mm)	5.74
Charging current (A)	1.7 galvanostatic mode and 0.1 potentiostatic mode
Discharging current (A)	1.7 and 2.2
Voltage cut off limit (V)	4.10/cell during charge and 3.00/cell during discharge

Technology Co. Ltd. China. The thermo-physical properties of the paraffin are listed in Table 4.

The thermal management performance of lithium ion batteries using graphene coated nickel foam was compared with four cases: nickel foam, paraffin wax, nickel foam saturated with paraffin wax and graphene coated nickel foam saturated with paraffin wax. Paraffin wax was infiltrated into the nickel foam and graphene coated nickel foam as shown in Fig. 4 (a). All the foams (nickel foam, nickel foam saturated with paraffin wax, GcN foam and GcN foam saturated with paraffin wax) were wrapped (single wrap) around individual battery cells as shown in the schematic diagram, Fig. 3 (a). This wrapping ensured compactness of the battery pack. In this way, the total weight for large power applications can also be reduced.

4.2. Testing of battery pack

The battery surface temperature was measured against five materials: (a) nickel foam, (b) paraffin wax, (c) nickel foam saturated with paraffin wax, (d) graphene coated nickel foam and (e) graphene coated nickel foam saturated with paraffin wax. Three T-type thermocouples (accuracy ~ 0.1 °C) were used to track the battery surface temperature. The position of the thermocouple was at the center of the first, third and fifth battery cells as shown in Fig. 3 (c). The battery pack was placed inside a container with dimension of 170 mm × 170 mm x 210 mm (L x W x H). The temperature of this container was controlled by an isothermal water bath as shown in Fig. 3(d). This temperature was traced by one separate T-type thermocouple. The charging of the battery pack was carried out at 1.7 A in galvanostatic mode with a voltage cut off limit of 4.1 V per cell, and then at potentiostatic mode with a current cut off of 100 mA per cell. The resting period followed the charging phase until the battery pack temperature dropped to the initial temperature. The discharge current for the battery pack was 1.7 A and 2.2

Table 4
Thermo-physical properties of the PCM.

Thermo-physical property	Value
Thermal conductivity (W/(m.K))	0.19
Density (kg/m^3)	880 solid state; 760 liquid state
Specific heat capacity (J/(kg.K))	2.3
Melting temperature range (°C)	38–41

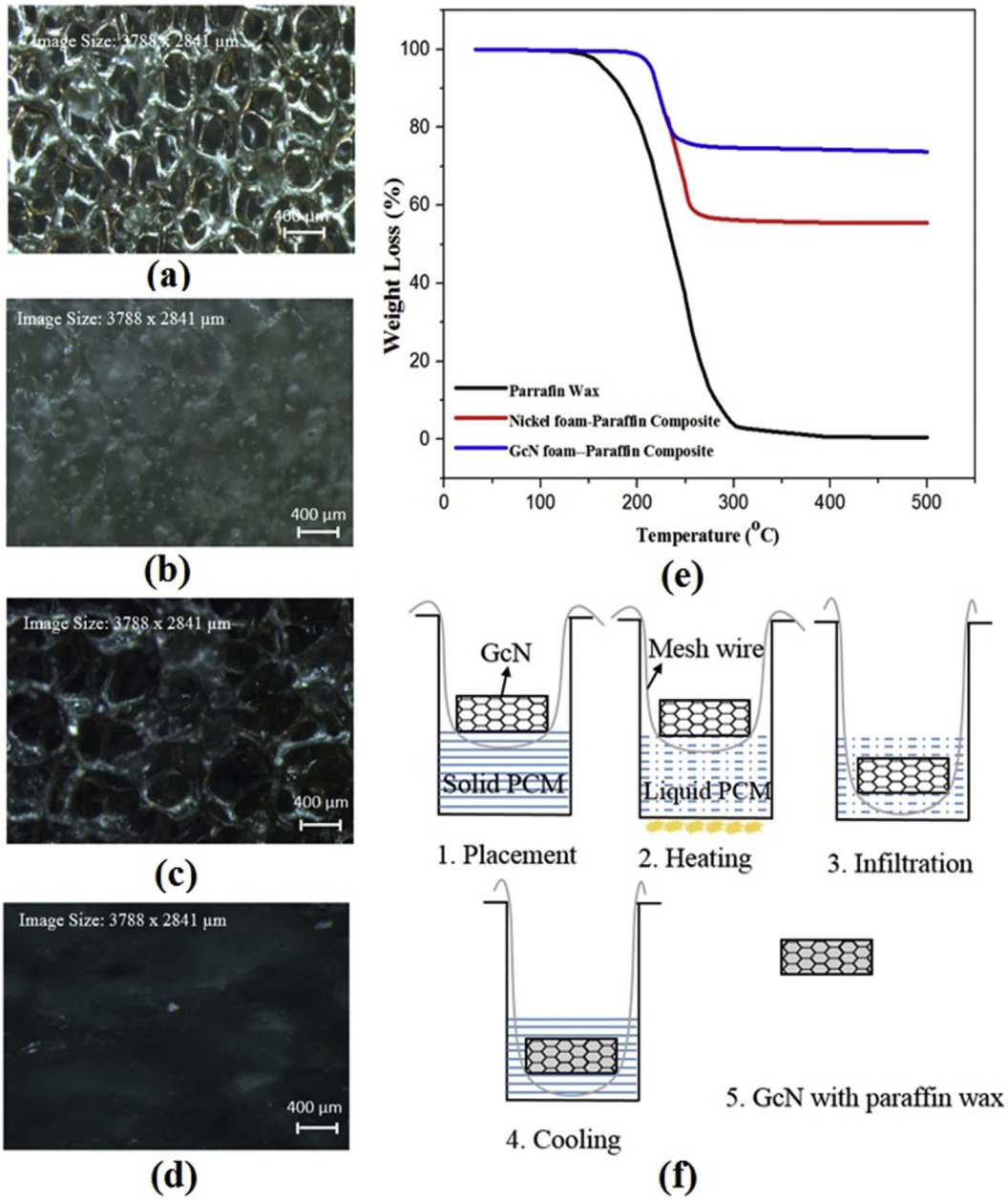

Fig. 4. Optical images of (a) nickel foam (12.7 PPI) (b) nickel foam saturated with paraffin wax (c) graphene coated nickel foam (d) graphene coated nickel foam saturated with paraffin wax (e) TGA analysis of the paraffin wax and composite (f) infiltration of paraffin wax into metal foams.

A. The discharge voltage cut off limit was 3 V per cell. Lastly, the temperature was allowed to fall to the initial temperature to complete the whole cycle. Experiments were conducted in different surrounding conditions (i.e. 25 °C, 30 °C and 33 °C). These temperature conditions were chosen to study the effects of different states (i.e. solid, liquid) of paraffin wax on the battery surface temperature. The charging and discharging of the battery pack was carried out by a Charge/discharge module (HYPERION EOS 720I NET3 AD) with an accuracy of 0.1%. The battery surface temperature was recorded by a data acquisition system (National Instruments NI 9213 with NI USB-9162, thermocouples and computer) after every 30 s. A schematic diagram of the experimental setup (charge/discharge module along with battery pack and isothermal water bath) is shown in Fig. 3 (d).

5. Results and discussion

5.1. Foam/paraffin composites morphologies

Fig. 4 (a) and (b) show the morphologies of the nickel foam before and after infiltration with paraffin wax. Similarly, Fig. 4 (c) and (d) show the morphologies of graphene coated nickel foam before and after infiltration with paraffin wax. The paraffin wax was observed to be compatible with the above-mentioned metal foams. The mass percentages of paraffin wax in nickel foam saturated with paraffin wax and graphene coated nickel foam saturated with paraffin wax were 84% and 71% respectively. The mass of paraffin wax infiltrated into the metal foam was calculated by measuring the difference in mass of the metal (nickel and graphene coated nickel) foam before and after infiltrating it with paraffin wax. Thermal stability is the most important term for PCM composites. The thermal stability of the composites and paraffin wax was measured by carrying out thermogravimetric analysis (TGA) as

shown in Fig. 4 (e). Paraffin wax started to lose weight at about 133 °C. The compatibility between the foams and the paraffin wax is strong as indicated by the higher weight loss starting temperature. The paraffin wax at the top surface of the composite solidifies first due to the direct contact with air. So, the paraffin wax inside the container will solidify from the top to the bottom in this study. And also, during the cooling phase, the paraffin wax inside the graphene coated nickel foam solidifies quickly from the top surface due to the higher thermal conductivity as compared to paraffin wax inside nickel foam. The top solidified paraffin wax prevents more paraffin entering the graphene coated nickel foam from the top. That is why the graphene coated nickel foam has a less percentage of paraffin wax. The top solidified paraffin wax prevents more paraffin entering the graphene coated nickel foam from top as shown in Fig. 4 (f). The bottom and lateral side of the graphene coated nickel foam remains in contact with the liquid paraffin and the paraffin enters the foam from both sides. The nickel foam saturated with paraffin wax has a lower thermal conductivity, so the paraffin solidifies slowly from the top and more paraffin wax would enter from the top surface. That is why more mass percentage of the paraffin has entered into the nickel foam. A change in color of the metal foam is observed, representing the coating of graphene on the nickel foam. The impregnation ratio was calculated to determine the percentage of nickel foam and graphene coated nickel foam saturated with paraffin wax. The impregnation ratio, β was calculated using the following relation [27].

$$\beta = \frac{\Delta M}{\varepsilon V \rho_{pcm}}, \tag{5}$$

where β is the impregnation ratio, ΔM is the difference in mass (kg) of the graphene coated metal foam and the graphene coated metal foam saturated with paraffin wax. ε is the porosity of the metal foam, V is the total volume (m^3) of the graphene coated metal foam and ρ_{pcm} is the density (kg/m^3) of the paraffin wax infiltrated into the graphene coated metal foam. The impregnation ratios in the case of nickel foam and graphene coated nickel foam saturated with paraffin wax were 90% and 83% respectively.

5.2. Thermal characterization of the composites

5.2.1. Thermal conductivities of the metal (nickel and graphene coated nickel) foam paraffin composites

Pure paraffin wax as a phase change material has the disadvantage of lower thermal conductivity (~0.1–~0.3 W/(m.K)). The thermal conductivity of the pure paraffin wax used in this study is 0.19 W/(m.K) measured by the equipment shown in Fig. 2. The thermal conductivity of this PCM was enhanced by infiltrating it into metal (nickel and graphene coated nickel) foams. Nickel/paraffin composite enhanced the thermal conductivity of pure paraffin by 6 times (~1.2 W/(m.K)) at room temperature (i.e. 25 °C), as is evident from Fig. 5. This increase in thermal conductivity was further enhanced by 23 times (~4.6 W/(m.K)) at a room temperature condition after infiltrating the PCM into the graphene coated nickel foam. Graphene/graphite/carbon foam are suitable candidates in enhancing the thermal conductivity of PCM due to their high thermal conductivity and low densities [40]. The thermal conductivity was enhanced significantly by many times due to the strong thermal coupling of the graphene with the paraffin wax [14]. The experiments to measure thermal conductivity were repeated six times and very little deviation was observed. The higher thermal conductivity of the paraffin wax composite will aid in dissipating the heat from source at a rapid rate.

5.2.2. Latent heat of nickel foam/paraffin composite and graphene coated nickel foam saturated with paraffin wax

The latent heat of pure paraffin, nickel foam/paraffin composite and graphene coated nickel foam saturated with paraffin wax are shown in Fig. 5. The deviations in temperature measurement using the DSC Q1000 is 0.2 °C ± 1% while the uncertainty in latent heat measurement is estimated to be 3%. This was obtained by numerical integration of the area under the two DSC peaks. It can be seen that the latent heat of the pure paraffin was 143 kJ/kg, while that of nickel foam/paraffin composite and graphene coated nickel foam saturated with paraffin wax were 120 kJ/kg and 99 kJ/kg respectively. The latent heat of nickel foam/paraffin and graphene coated nickel foam/paraffin were lowered by about 16% and 31% respectively. This decrease is attributed to the fact that mass fraction of the pure paraffin is decreased in metal (nickel and graphene coated nickel) foam/PCM composites due to small cavities, thus decreasing the latent heat of the metal (nickel and graphene coated nickel) foam/PCM composite.

5.2.3. Phase change behavior of nickel foam/paraffin composite and graphene coated nickel foam saturated with paraffin wax

The shift in phase change temperature (PCT) of PCM is observed after infiltration of PCM into the metal (nickel and graphene coated nickel) foam. The freezing/melting curves of metal (nickel and graphene coated nickel) foams saturated with PCM are shown in Fig. 6 (a) and (b) respectively. The cooling process is shown by the negative heat flow while the positive heat flow represents the heating process. The main peak represents the solid-liquid phase change while the neighboring small peak represents the solid-solid transition peak. The extrapolated onset temperature and peak temperature of the metal foam/PCM in case of freezing shows a decrease in temperature. The melting of the paraffin wax starts at a temperature of 37 °C. The extrapolated onset temperature and peak temperature of metal (nickel and graphene coated nickel) foam/PCM composite in the case of the melting process shows a shift towards higher temperature. Strong interactions and compatibility exist between the metal foam and paraffin wax. The shift in the starting and ending temperature of the freezing and melting temperature of the composites is due to this strong interaction [37]. The melting temperature is associated with interfacial interaction between the solid and liquid states and the properties of the two phases (solid and liquid) as is evident from the Gibbs-Thomson equation [41].

$$T_m^{\infty} - T_{m(r)} = \frac{4\gamma_{sl} T_m^{\infty}}{r \Delta H_f \rho_s}, \tag{6}$$

where T_m is the melting point of paraffin wax (°C), the surface energy at the solid-liquid interface is represented by γ_{sl} (J/m^2), H_f is the fusion enthalpy per unit mass (J/kg), r is the radius between the metal foam and nucleating phase of paraffin wax (m) and ρ_s is the density of the

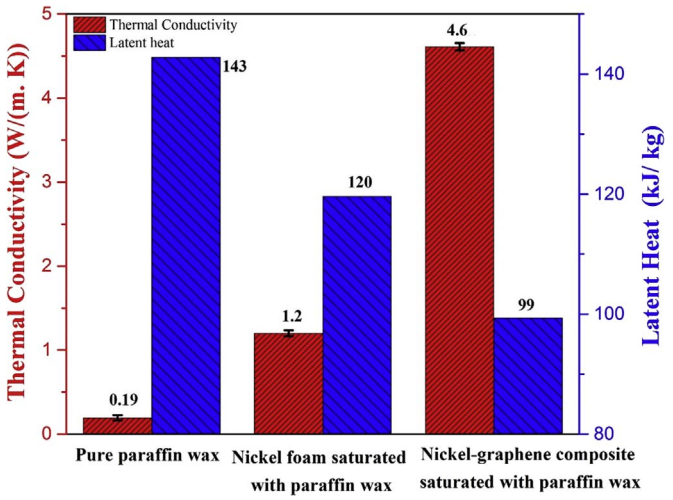

Fig. 5. Thermal conductivity (at 25 °C) and Latent heat of pure paraffin wax, nickel foam saturated with paraffin wax and graphene coated nickel foam saturated with paraffin wax.

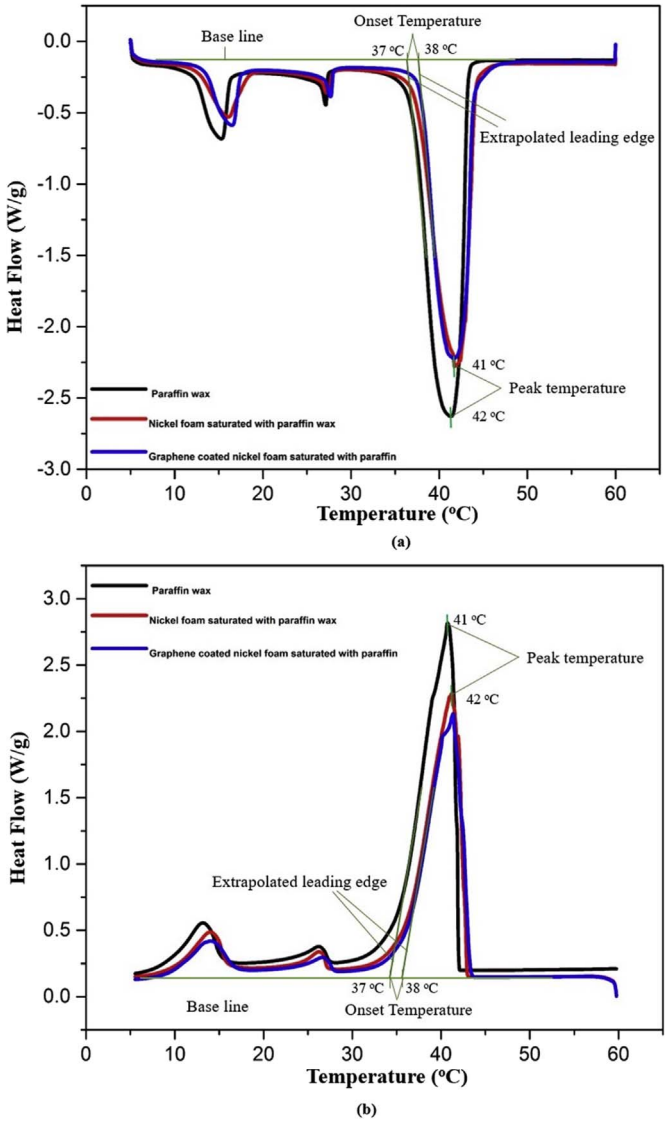

Fig. 6. DSC curves showing (a) freezing process (b) melting process of pure paraffin and metal (nickel/Graphene coated nickel) foams saturated with paraffin.

substrate (nickel foam and graphene coated nickel foam) (kg/m^3). The shifting in freezing and melting temperature is evident from eq. (6) as the melting temperature of the paraffin wax depends on the metal foam pore structure-solid interaction and metal foam pore structure-liquid interaction. The extrapolated onset and peak temperature for the melting process in the case of nickel foam and graphene coated nickel foam saturated with paraffin wax is increased as compared to pure paraffin wax due to the strong interaction between the phase change material and composite foams.

5.2.4. Specific heat capacities of metal (nickel and graphene coated nickel) foam/paraffin composites

The specific heat capacities of nickel foam/graphene coated nickel foam/paraffin composites both in solid and liquid state are shown in Table 5. The specific heat capacities in the solid and liquid state were measured at an average value in the temperature range of 23–28 °C and 55–60 °C respectively. The specific heat capacity in a liquid state is slightly higher than that in the solid state. Also, the specific heat capacity of the metal (nickel and graphene coated nickel) foam/paraffin composite in both states is smaller compared with that of pure paraffin, since the specific heat capacity of the metal (nickel and graphene coated nickel) skeleton is smaller than that of the pure PCM.

Moreover, the electrical conductivity of the composites is determined using the four-probe method. The results are shown in the Table 6.

The safety circuit was connected with a battery pack to prevent short circuit due to conductive nature of the composites as shown in Fig. 3 (b).

5.3. Thermal management of Li-ion batteries using graphene coated nickel foam saturated with paraffin wax

The battery surface temperature was tested against five materials (a) nickel foam, (b) graphene coated nickel foam, (c) paraffin wax, (d) nickel foam saturated with paraffin wax and (e) graphene coated nickel foam saturated with paraffin wax. The battery pack was placed inside a container with dimensions of 170 mm × 170 mm x 210 mm. A thermostatic water bath was used to maintain different stable temperatures (i.e. 25, 30, 33 °C) in the container as shown in the schematic diagram (Fig. 3 (d)). The battery temperature profile of cell number 3 under 1.7 A and 2.2 A is shown in Fig. 7 and Fig. 8 respectively. The battery temperature profile of cell number 3 at surrounding temperatures of 25, 30, 33 °C is shown in Fig. 7 (a, b, c) and Fig. 8 (a, b, c) respectively. Cell 3 was chosen as it has the highest temperature rise being approximately at the center of the battery pack. Moreover, the peak temperature difference (between cell number 1 and cell number 3) inside the battery pack was less than 1%. At a 25 °C surrounding temperature, the battery surface temperature rose to 34 °C and 38 °C using nickel foam as the thermal management material under 1.7 A and 2.2 A discharge rate respectively. The heat generated by the battery was dissipated at a faster rate by wrapping nickel foam around the battery cells compared to the case with no nickel foam. However, when the battery cells were wrapped with graphene coated nickel foam, the temperature dropped to 34 °C and 36 °C under 1.7 A and 2.2 A discharge rate respectively at 25 °C surrounding temperature. This small decrease in temperature implies that the graphene growth on nickel foam has increased the heat dissipation rate through conduction. This minimum temperature drop using graphene coated nickel foam as compared to nickel foam was also evident even at 30, 33 °C surrounding temperatures. It is worth mentioning here that a higher temperature rise was observed when the battery pack was discharged at a higher surrounding temperature under the same discharge rate. A temperature rise of 9 °C at the surrounding temperature of 25 °C was observed but temperature rise is 16 °C for the battery with a surrounding temperature of 30 °C for the 1.7 A discharge rate. The degradation rate is increased at the higher temperatures due to an increase in electrode wetting and the electrolyte conductivity properties of the battery cells. This abrupt increase in temperature poses a serious threat to lithium ion battery performance. Surrounding the battery cells with nickel foam and/or graphene coated nickel foam may create problems during summer as the surrounding temperatures are much higher.

It was well established that the battery discharge temperature first rises linearly until a 70% state of charge (SOC) level is reached and drops till the SOC drops to 30% and then rises linearly again [42]. As a result, the battery temperature profile using nickel foam and graphene coated nickel foam showed a slight decline trend during the middle of

Table 5
Specific heat capacities of pure paraffin and metal (nickel/Graphene coated nickel) foams/paraffin composites.

	C_{ps} (J/(g.K)) (23–28 °C)	C_{pl} (J/(g.K)) (55–60 °C)
Pure paraffin wax	2.3	2.5
Nickel foam	0.8	–
Graphene coated nickel foam	1.1	–
Nickel foam/paraffin composite	1.7	2
Graphene coated nickel/paraffin composite	1.6	1.8

Table 6
Electrical conductivity of the composites.

Composite	Electrical conductivity (S/cm)
Nickel foam/paraffin composite	1.4×10^3
Graphene coated nickel/paraffin composite	1.5×10^3

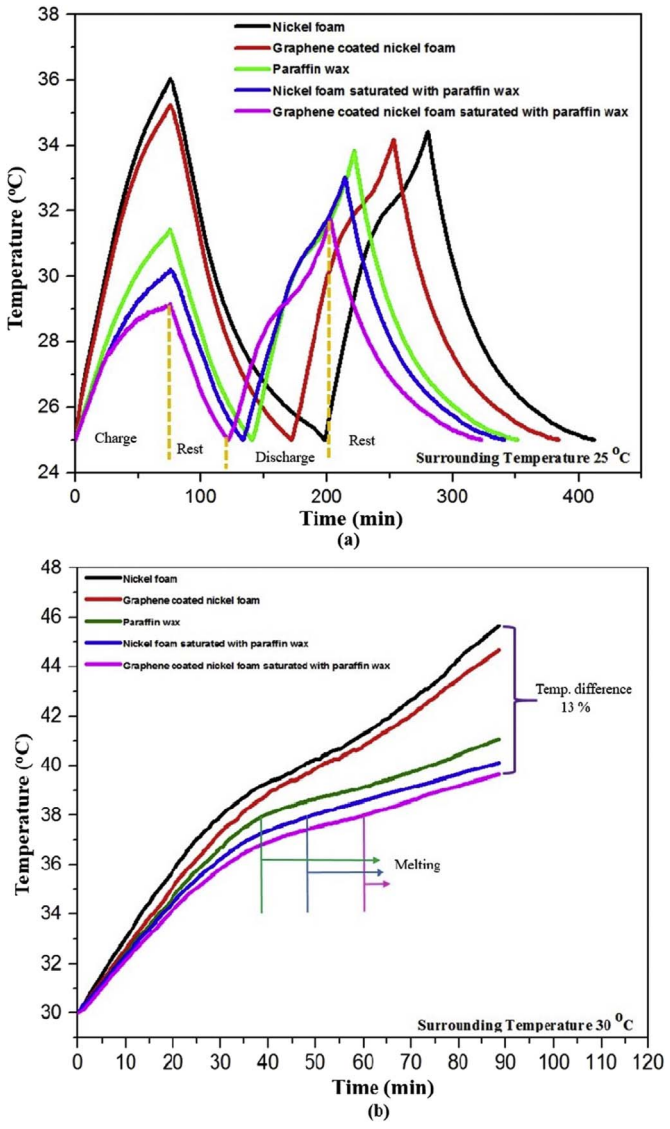

Fig. 7. Temperature variation with time for all dissipation materials under 1.7 A discharge current and at battery pack surrounding temperatures of (a) 25 °C; (b) 30 °C; and (c) 33 °C.

the discharge process as is evident by Fig. 7(a–c). The temperature dropped significantly when the battery pack was surrounded by a passive thermal management system i.e. paraffin wax and metal (nickel and graphene coated nickel) foam saturated with paraffin wax. The battery surface temperature with paraffin as the thermal management material reached 34 °C, 35 °C under a discharge rate of 1.7 A and 2.2 A respectively and at surrounding temperature of 25 °C. The paraffin wax was not melted at the surrounding temperature of 25 °C. However, it melted at surrounding temperatures of 30 and 33 °C. The solid, melting and liquid phase of paraffin wax is evident from Fig. 7 (c) and Fig. 8 (c). The heat generated by the battery pack was dissipated through thermal conduction and thermal convection during the solid and liquid phase of paraffin wax respectively. This heat dissipation was further enhanced

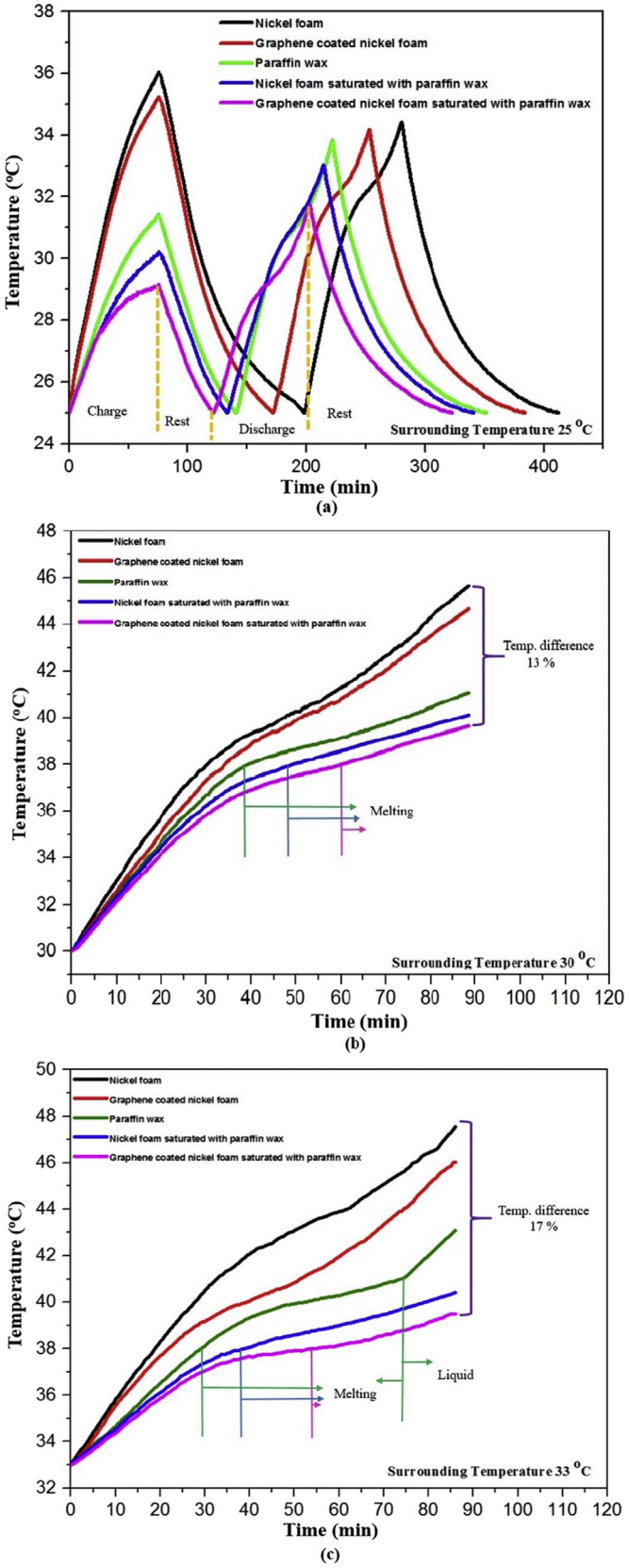

Fig. 8. Temperature variation with time for all dissipation materials under 2.2 A discharge current and at battery pack surrounding temperatures of (a) 25 °C; (b) 30 °C; and (c) 33 °C.

by infiltrating the paraffin wax into the nickel foam and graphene coated nickel foam. This is due to the thermal conductivity of the pure paraffin wax being increased after saturating the nickel foam and graphene coated nickel foam with paraffin. The battery surface temperature was 40 °C and 43 °C after enveloping the battery cells in nickel foam saturated with paraffin under 1.7 A and 2.2 A, respectively, at a 30 °C surrounding temperature. The paraffin just melted under 1.7 A discharge rate while the liquid phase of paraffin was observed under 2.2 A discharge rate. As the battery cells were provided with a thermal management material of graphene coated nickel foam saturated with paraffin wax, the battery surface temperature was 39 °C (about 17% less than that of nickel foam) under 1.7 A discharge rate and at a surrounding temperature of 33 °C. The melting of paraffin was observed in this case. During melting, the temperature rose smoothly as the heat was being stored in the form of latent heat. Heat dissipation took place through heat convection after melting. The battery surface temperature after being enveloped by graphene coated nickel foam saturated by paraffin wax was 11% less compared to that of nickel foam as the thermal management under a higher discharge rate i.e. 2.2 A. A 17% lower temperature suggests that graphene coated nickel saturated with paraffin wax can prove to be a viable option with respect to thermal management of lithium ion batteries. It should be noted that the paraffin stays inside the metal foam during the phase change since it is well-known that paraffin in a molten state will be fixed by capillary forces in an open-cell composite structure [43]. It should also be noted that liquid paraffin flows to the top surface due to the density variation between liquid and solid paraffin during the melting process [44]. Since there was no shaking, vibrating, or oscillating of the battery pack, it is strongly believed that the paraffin would not leak out. Organic phase change materials (i.e. paraffin waxes, erythritol, etc.) have shown a reasonably good thermal reliability in view of changes in thermal properties with respect to thermal cycling [45]. In our experiments, each composite was cycled at least 24 times for battery thermal management systems (i.e. 4 times for each specific discharge current and ambient condition) and an almost negligible deviation (i.e. about ~1% difference in battery surface temperature is observed using graphene coated nickel foam saturated with paraffin wax under 2.2 A discharge current and 33 °C ambient temperature among all 4 cycled measured temperature values). So, it is believed that there is no significant reduction in the thermal properties of the composite materials even after many continuous thermal cycles.

5.4. Temperature uniformity

This temperature difference along the battery pack will result in loss of battery life due to performance drops and safety hazards. A uniform temperature distribution along the battery pack is essential to achieve higher capacity utilization and lower capacity fading. The temperature difference between cells number 1 and 3 with the thermal management system of nickel foam and graphene coated nickel foam saturated with paraffin wax under 2.2 A discharge current is shown in Fig. 9 (a) and 9 (b), respectively. With the case of nickel foam as thermal management system, a temperature difference of 2 °C is obtained as shown in Fig. 9 (a). The results shown are at a surrounding ambient temperature of 33 °C. This temperature difference is reduced to a greater extent, when graphene coated nickel foam saturated with paraffin wax is used. For the graphene coated nickel foam saturated with paraffin wax composite, a temperature difference of 0.7 °C is obtained. This small temperature difference (0.7 °C) between cell 1 and cell 3 confirms that the heat is conducted efficiently throughout the graphene coated nickel foam saturated with paraffin wax composite, also proving that the PCM is uniformly distributed in the pores of the metal foam.

6. Conclusions

The graphene coated nickel foam was prepared using the chemical vapor deposition technique. The thickness of the graphene layer on the nickel foam was 1–2 nm. The paraffin wax as a phase change material was infiltrated into the graphene coated nickel foam. The thermal characterization of graphene coated nickel foam saturated with paraffin wax and its application for the thermal management of lithium ion batteries were studied. The key findings are summarized below.

1. The thermal conductivity of graphene coated nickel foam saturated with paraffin wax as well as nickel foam saturated with paraffin wax was measured using laser flash methodology. The paraffin wax was infiltrated into the metal foams. The result indicates that the graphene coated nickel foam improved the thermal conductivity of the pure paraffin by 23 times while the nickel foam enhanced the thermal conductivity of pure paraffin by 6 times.
2. The shifting in the melting temperature as well as the freezing temperature of the graphene coated nickel foam saturated with paraffin wax was observed and compared to pure paraffin. The melting and freezing temperature of the composite material (nickel foam/graphene coated nickel foam saturated with paraffin wax) increased and decreased respectively as compared to those of

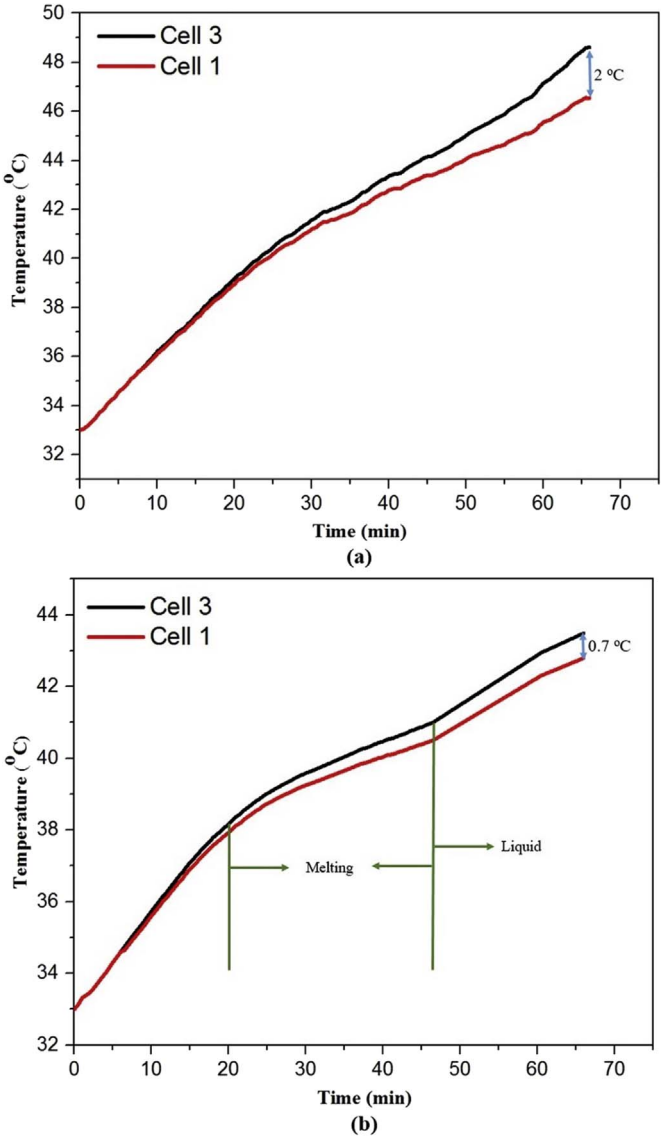

Fig. 9. Temperature difference between battery cells number 1 and 3 for (a) nickel foam (b) graphene coated nickel foam saturated with paraffin composite as a cooling mode under 33 °C ambient conditions and 2.2 A discharge current.

paraffin. This shift in the melting temperature of paraffin wax depends on the metal foam pore structure-solid interaction and metal foam pore structure-liquid interaction.

3. The latent heat of the graphene coated nickel foam saturated with paraffin wax was decreased by 30% as compared to the latent heat of pure paraffin wax. This is due to a decrease in the mass fraction of the pure paraffin inside the graphene coated nickel foam. The decrease in the amount of paraffin wax is due to the metal foam's small cavities. The specific heat capacity of the nickel foam saturated with phase change material is 16% and 12% smaller as compared to pure paraffin in solid and liquid states respectively, while the specific heat capacity of the graphene coated nickel saturated with phase change material is 35% and 34% smaller as compared to pure paraffin in solid and liquid states respectively. The reason for this is the smaller specific heat capacity of the metal skeleton (nickel foam and nickel-graphene foam) as compared to pure PCM.
4. Last, this study includes the application (i.e. the thermal management of the lithium ion batteries) of the developed material. Four additional thermal management materials i.e. nickel foam, graphene coated nickel foam, paraffin wax and nickel foam saturated with paraffin wax are also studied and compared. The rise in battery surface temperature is 17% lower after using graphene coated nickel foam saturated with paraffin wax as the thermal management material under 1.7 A discharge current as compared to nickel foam.

Acknowledgments

The authors appreciate the Hong Kong Research Grant Council for providing research fund via account 16202517, Science and Technology Planning Project of Guangdong Province via account 2017A050506050, Guangzhou Science and Technology Program via account 2016201604030056, Science and Technology Program of Nansha District via account 2015KF029 and Postdoc Station at Guangzhou Nansha via account 180852. We also acknowledge Prof. Lawrence Li and Mr. Abdul Wasy Zia for permitting use of the equipment facilities from The City University of Hong Kong. And also, the first author gratefully recognizes the Higher Education Commission (HEC) of Pakistan for financing his higher studies under HRDI-UESTPs (Phase 1-Batch 3) scholarship scheme.

References

[1] O. Egbue, S. Long, Barriers to widespread adoption of electric vehicles: an analysis of consumer attitudes and perceptions, Energy Policy 48 (2012) 717–729.
[2] T.E. Lipman, M.A. Delucchi, Hybrid-electric vehicle design retail and life cycle cost analysis final report, (2003) http://www.its.ucdavis.edu/.
[3] D. Linden, T.B. Reddy, Handbook of batteries, third ed., (2002) New York.
[4] T.L. Pourpoint, V. Velagapudi, I. Mudawar, Y. Zheng, T.S. Fisher, Active cooling of a metal hydride system for hydrogen storage, Int J Heat Mass Transf 53 (2010) 1326–1332.
[5] F. He, L. Ma, Thermal management of batteries employing active temperature control and reciprocating cooling flow, Int J Heat Mass Transf 83 (2015) 164–172.
[6] X. Duan, G.F. Naterer, Heat transfer in phase change materials for thermal management of electric vehicle battery modules, Int J Heat Mass Transf 53 (2010) 5176–5182.
[7] H. So, A.P. Pisano, Micromachined passive phase-change cooler for thermal management of chip-level electronics, Int J Heat Mass Transf 89 (2015) 1164–1171.
[8] T.H. Tran, S. Harmand, B. Desmet, S. Filangi, Experimental investigation on the feasibility of heat pipe cooling for HEV/EV lithium-ion battery, J Power Sources 63 (2014) 551–558.
[9] A. Greco, D. Cao, X. Jiang, H. Yang, A theoretical and computational study of lithium-ion battery thermal management for electric vehicles using heat pipes, J Power Sources 257 (2014) 344–355.
[10] S.K. Mohammadian, S.M. Rassoulinejad-Mousavi, Y. Zhang, Thermal management improvement of an air-cooled high-power lithium-ion battery by embedding metal foam, J Power Sources 296 (2015) 305–313.
[11] J. Zhao, Z. Rao, Y. Li, Thermal performance of mini-channel liquid cooled cylinder based battery thermal management for cylindrical lithium-ion power battery, Energy Convers Manag 103 (2015) 157–165.
[12] Z. Rao, S. Wang, A review of power battery thermal energy management, Renew Sustain Energy Rev 15 (2011) 4554–4571.
[13] B. Zalba, J.M. Marin, L.F. Cabeza, H. Mehling, Review on thermal energy storage with phase change: materials, heat transfer analysis and applications, Appl Therm Eng 23 (2003) 251–283.
[14] P. Goli, S. Legedza, A. Dhar, R. Salgado, J. Renteria, A.A. Balandin, Graphene-enhanced hybrid phase change materials for thermal management of Li-ion batteries, J Power Sources 248 (2014) 37–43.
[15] R. Kizilel, R. Sabbah, J.R. Selman, S. Al-Hallaj, An alternative cooling system to enhance the safety of Li-ion battery packs, J Power Sources 194 (2009) 1105–1112.
[16] M. Aadmi, M. Karkri, M. El Hammouti, Heat transfer characteristics of thermal energy storage for PCM (phase change material) melting in horizontal tube: numerical and experimental investigations, Energy 85 (2015) 339–352.
[17] L. Zhang, J. Zhu, W. Zhou, J. Wang, Y. Wang, Thermal and electrical conductivity enhancement of graphite nanoplatelets on form-stable polyethylene glycol/polymethyl methacrylate composite phase change materials, Energy 39 (2012) 294–302.
[18] T. Wang, S. Wang, W. Wu, Experimental study on effective thermal conductivity of microcapsules based phase change composites, Int J Heat Mass Transf 109 (2017) 930–937.
[19] J. Fukai, Y. Hamada, Y. Morozumi, O. Miyatake, Effect of carbon-fiber brushes on conductive heat transfer in phase change materials, Int J Heat Mass Transf 45 (2002) 4781–4792.
[20] T.K. Tullius, Y. Bayazitoglu, Temperature of a metallic nanoparticle embedded in a phase change media exposed to radiation, Int J Heat Mass Transf 93 (2016) 980–990.
[21] W.Q. Li, Z.G. Qu, Y.L. He, Y.B. Tao, Experimental study of a passive thermal management system for high-powered lithium ion batteries using porous metal foam saturated with phase change materials, J Power Sources 255 (2014) 9–15.
[22] A. Hussain, C.Y. Tso, C.Y.H. Chao, Experimental investigation of a passive thermal management system for high-powered lithium ion batteries using nickel foam-paraffin composite, Energy 115 (2016) 209–218.
[23] F. Samimi, A. Babapoor, M. Azizi, G. Karimi, Thermal management analysis of a Li-ion battery cell using phase change material loaded with carbon fibers, Energy 96 (2016) 355–371.
[24] R. Sabbah, R. Kizilel, J.R. Selman, S. Al-Hallaj, Active (air-cooled) vs. passive (phase change material) thermal management of high power lithium-ion packs: limitation of temperature rise and uniformity of temperature distribution, J Power Sources 182 (2008) 630–638.
[25] S.A. Khateeb, S. Amiruddin, M. Farid, J.R. Selman, S. Al-Hallaj, Thermal management of Li-ion battery with phase change material for electric scooters: experimental validation, J Power Sources 142 (2005) 345–353.
[26] R. Addou, A. Dahal, P. Sutter, M. Batzill, Monolayer graphene growth on Ni(111) by low temperature chemical vapor deposition, Appl Phys Lett 100 (2012).
[27] X. Xiao, P. Zhang, M. Li, Preparation and thermal characterization of paraffin/metal foam composite phase change material, Appl Energy 112 (2013) 1357–1366.
[28] J. Lahiri, T.S. Miller, A.J. Ross, L. Adamska, I.I. Oleynik, M. Batzill, Graphene growth and stability at nickel surfaces, New J Phys 13 (2011).
[29] A. Reina, X. Jia, J. Ho, D. Nezich, H. Son, V. Bulovic, et al., Large area, few-layer graphene films on arbitrary substrates by chemical vapor deposition, Nano Lett 9 (2009) 30–35.
[30] Y. Zhao, Z. Wu, Y.-F. Zhang, S.L. Bai, Thermal conductivity of 3D graphene filled polymer, 10th international conference on composite science and technology, 2015, pp. 1–8.
[31] X. Zhao, Q. Zhang, D. Chen, P. Lu, Enhanced mechanical properties of graphene-based polyvinyl alcohol composites, Macromolecules 43 (2010) 2357–2363.
[32] K.M.F. Shahil, A.A. Balandin, Graphene-multilayer graphene nanocomposites as highly efficient thermal interface materials, Nano Lett 12 (2012) 861–867.
[33] K.M.F. Shahil, A.A. Balandin, Thermal properties of graphene and multilayer graphene: applications in thermal interface materials, Solid State Commun 152 (2012) 1331–1340.
[34] D.L. Nika, A.A. Balandin, Phonon transport in graphene, J Physic 24 (2012) 1–41.
[35] Z. Ren, N. Meng, K. Shehzad, Y. Xu, S. Qu, B. Yu, et al., Mechanical properties of nickel-graphene composites synthesized by electrochemical deposition, Nanotechnology 26 (2015) 65706.
[36] C. Zhou, J.A. Szpunar, X. Cui, Synthesis of Ni/Graphene nanocomposite for hydrogen storage, ACS Appl Mater Interfaces 8 (2016) 15232–15241.
[37] D. Zhang, S. Tian, D. Xiao, Experimental study on the phase change behavior of phase change material confined in pores, Sol Energy 81 (2007) 653–660.
[38] L.M. Malard, M.A. Pimenta, G. Dresselhaus, M.S. Dresselhaus, Raman spectroscopy in graphene, Phys Rep 473 (2009) 51–87.
[39] W.J. Parker, R.J. Jenkins, C.P. Butler, G.L. Abbott, Flash method of determining thermal diffusivity heat capacity and thermal conductivity, J Appl Phys 32 (1961) 1679–1984.
[40] M. Moeini Sedeh, J.M. Khodadadi, Thermal conductivity improvement of phase change materials/graphite foam composites, Carbon N Y 60 (2013) 117–128.
[41] L.D. Gelb, K.E. Gubbins, R. Radhakrishnan, M. Sliwinska-Bartkowiak, Phase separation in confined systems, Rep Prog Phys 63 (2000) 727.
[42] S. Goutam, J.M. Timmermans, N. Omar, P. Van denBossche, J. VanMierlo, Comparative study of surface temperature behavior of commercial li-ion pouch cells of different chemistries and capacities by infrared thermography, Energies 8 (2015) 8175–8192.
[43] C. Wang, T. Lin, N. Li, H. Zheng, Heat transfer enhancement of phase change composite material: copper foam/paraffin, Renew Energy 96 (2016) 960–965.
[44] J. Meinert, Cellular metals and composites for an optimization of the loading and re-loading behavior of thermal storages, 4th international renewable energy storage conference, fraunhofer institute of manufacturing and applied materials, Dresden Branch Lab, Winterbergstrasse, 2009, p. 28.
[45] A. Shukla, D. Buddhi, R.L. Sawhney, Thermal cycling test of few selected inorganic and organic phase change materials, Renew Energy 33 (2008) 2606–2614.

[46] Z. Wang, Z. Zhang, L. Jia, L. Yang, Paraffin and paraffin/aluminum foam composite phase change material heat storage experimental study based on thermal management of Li-ion battery, Appl Therm Eng 78 (2015) 428–436.
[47] X. Xiao, P. Zhang, M. Li, Effective thermal conductivity of open-cell metal foams impregnated with pure paraffin for latent heat storage, Int J Therm Sci 81 (2014) 94–105.
[48] H. Ji, D.P. Sellan, M.T. Pettes, X. Kong, J. Ji, L. Shi, et al., Enhanced thermal conductivity of phase change materials with ultrathin-graphite foams for thermal energy storage, Energy Environ Sci 7 (2014) 1185.
[49] H. Fathabadi, High thermal performance lithium-ion battery pack including hybrid active-passive thermal management system for using in hybrid/electric vehicles, Energy 70 (2014) 529–538.